An Optimized Control Scheme for Reducing Conduction and Switching Losses in Dual Active Bridge Converters

Liu, Bochen; Davari, Pooya; Blaabjerg, Frede

Published in:
Proceedings of the IEEE Energy Conversion Congress and Exposition (ECCE 2018)

DOI (link to publication from Publisher):
10.1109/ECCE.2018.8557883

Publication date:
2018

Document Version
Accepted author manuscript, peer reviewed version

An Optimized Control Scheme for Reducing Conduction and Switching Losses in Dual Active Bridge Converters

Bochen Liu, Pooya Davari, Frede Blaabjerg
Department of Energy Technology
Aalborg University
Aalborg, Denmark
bli@et.aau.dk, pda@et.aau.dk, fbl@et.aau.dk

***Abstract*—An optimized switching control strategy to reduce the conduction and switching losses of the dual active bridge converter is presented in this paper. The control strategy can simultaneously reduce the root mean square value and average absolute value of the leakage inductor current, which are closely relevant to the conduction and switching losses of the semiconductor devices and high-frequency transformers. The optimization is conducted by regulating two manipulated variables on the basis of achieving zero-voltage switching for all switches in a wide voltage range as well as effectively reducing the power losses. An experimental prototype was implemented to validate the theoretical analysis and the feasibility of the proposed method. The experimental results revealed that the converter power losses can effectively be reduced and the overall system efficiency can be improved using the proposed control strategy.**

Keywords—dual active bridge, power losses, zero voltage switching

I. INTRODUCTION

The dual active bridge (DAB) converter is now widely used in many applications such as electric vehicles and distributed power systems to adapt different voltage levels and control the power flow among multiple energy sources [1]-[3]. Further advantages, such as having high efficiency, galvanic isolation and bidirectional power flow also make DAB converter as a potential candidate for the future charging systems and vehicle-to-grid (V2G) power transfer.

The DAB converters can operate efficiently when all switches can achieve zero-voltage switching (ZVS), but such efficient operation for the entire power range is only achievable when the voltage ratio is equal to one. If it deviates far from one, the converter efficiency will be greatly reduced in partial loading conditions and even the switches would be broken with excessive *dv/dt* caused by ZVS failure. In order to overcome this drawback, many improved modulation methods are introduced to extend the DAB soft-switching operating range, such as extended phase-shift (EPS) modulation [4], dual phase-shift (DPS) modulation [5], [6] and triple phase-shift (TPS) modulation [7], [8]. In the prior-art phase-shift modulation, the diagonal switches of each full bridge are switched in order to transfer the energy through the linked leakage inductor. Besides, these improved modulation methods generate the driving signals for each switch by adding extra degrees of freedom such that the duty cycle and phase-shift angle of the high-frequency output AC voltage for each full bridge can be also regulated online. Moreover, the converter efficiency and/or power density can be enhanced at the same time if proper optimization methods are applied in [9], but the control complexity is also increased owing to multiple control variables.

In order to further decrease the power degradation of the switches and to reduce the power losses, several hybrid modulation strategies are discussed in [10], [11]. However, the selection and calculation of the optimal modulation parameters are usually complex. On the other hand, minimizing the root mean square (RMS) current of the transformers is introduced in [12], [13] in order to reduce the overall conduction loss and improve the efficiency, but it is often addressed independent from the soft-switching technology for all switches. In fact, the conduction losses of the switches are more related to the average absolute value of the conduction current rather than the RMS value in some specific applications where the insulated gate bipolar transistors (IGBTs) are employed [14] instead of the metal oxide semiconductor field effect transistors (MOSFETs). Besides, as the zero-voltage switching in DAB converters commonly occurs at the instant of turning on, the turn-off switching losses should be also taken into account, especially when higher switching frequency operation is required. Thereby, minimizing the conduction and switching losses are of high importance to both silicon transistors and the new generation power semiconductors like Silicon Carbide (SiC) [15] and Gallium Nitride (GaN) devices [16].

This paper proposes a uniform control scheme to extract the optimal modulation parameters for dual-phase-shift modulation. With the proposed scheme, the conduction and switching losses of the switches and the intermediate transformer are reduced and all switches can achieve soft-switching in a wide voltage range. Firstly, the DAB operation modes are introduced in Section II, and then the conduction and switching losses model are discussed in Section III. Next, the optimized control scheme is explained in Section IV where a comprehensive analysis and comparison among different control schemes is implemented and verified with simulations. In Section V, experimental results are presented to validate the effectiveness of the proposed control scheme. Finally, conclusions are drawn in Section VI.

II. DAB OPERATION

A DAB converter consisting of two full bridges (HB_1, HB_2) and a high-frequency transformer is shown in Fig. 1. Here, the direction of the power flow is from HB_1 to HB_2 and the converter is assumed to work in voltage boosting mode, namely $V_2>V_1/n$, where n is turns ratio of the isolated transformer. In order to simplify the analysis, all quantities are normalized using the base values as shown in (1) and the voltage ratio k is introduced as V_1/nV_2, which is within (0, 1).

$$P_b = \frac{(nV_1)^2}{8Lf_s} \qquad I_b = \frac{n^2V_1}{8Lf_s} \qquad V_b = V_2 \tag{1}$$

P_b, I_b and V_b are the benchmark power, current and voltage, respectively. V_1, V_2 and f_s denotes the input, output dc voltage and the switching frequency, respectively. L is the total inductance referred to the primary side, consisting of the transformer leakage inductor and the auxiliary inductor. The magnetizing inductance of the transformer is considered to be much larger than its leakage inductance. Notably, in order to flexibly adjust the leakage inductance value, an auxiliary inductor is introduced as a part of the equivalent total leakage inductance and it is in series with the primary high-voltage winding to lower the induced additional power losses.

The typical waveforms of the DAB converter with dual-phase-shift (DPS) modulation are illustrated in Fig. 2. The cross switches S_2 and S_3 in the primary full bridge operate synchronously while the switches cascaded in one leg (e.g. S_1 and S_3) operate oppositely and a dead time is introduced in order to avoid short circuit. Thus a 50% duty cycle two-level voltage v_p is generated in the primary full-bridge HB_1. Differently, for the secondary full bridge HB_2, taking the switching signal of S_2 as the reference, the cross switches S_6 and S_7 operate with a shifted angle β_1 and β_2, respectively, resulting in a three-level voltage v_s.

According to whether the falling edge of v_s leads or lags the falling edge of v_p, the DAB converter has two operation modes, namely Mode I as shown in Fig. 2(a) and Mode II as shown in Fig. 2(b). Therein, φ is the phase-shift angle between v_p and v_s, and α represents the duty cycle angle of v_s. The relationship between α, φ and β_1, β_2 can be expressed as:

$$\alpha = \pi - \beta_2 - \beta_1 \qquad \varphi = \frac{\beta_2 - \beta_1}{2} \tag{2}$$

$$\alpha = \pi - \beta_2 - \beta_1 \qquad \varphi = \frac{\beta_2 + \beta_1}{2} \tag{3}$$

(2) and (3) corresponds to Mode I and Mode II, respectively. Therefore, α and φ can be regulated by β_1 and β_2 for both modes. For simplification, D_α and D_φ are defined as:

$$D_\alpha = \frac{\alpha}{\pi} \qquad D_\varphi = \frac{\varphi}{\pi} \tag{4}$$

limited in the range of [0, 1] and [0, 0.5] for D_α and D_φ, respectively. Then the boundary of Mode I and Mode II can be obtained:

$$D_\alpha = 1 - 2D_\varphi \tag{5}$$

which means that if D_α <1-2D_φ, the DAB converter would work in Mode I, otherwise the converter would work in Mode II.

In addition, the secondary current i_s is shaped by the voltage drop on the leakage inductor, that is:

$$\frac{L}{n}\frac{di_s}{dt} = v_p - nv_s \tag{6}$$

So the normalized secondary current based on the switching instant can be derived using (6) following the operating waveforms shown in Fig. 2, as expressed by (7) and (8). In addition, the waveforms of the input and output current (i_1, i_2) of HB_1 and HB_2 are also illustrated in Fig. 2.

$$\text{Mode I} \begin{cases} i_s(t_0) = -\dfrac{2}{nV_1}(k - D_\alpha) \\ i_s(t_2) = \dfrac{2}{nV_1}\left[(1-k)D_\alpha + 2kD_\varphi\right] \\ i_s(t_4) = \dfrac{2}{nV_1}\left[(k-1)D_\alpha + 2kD_\varphi\right] \end{cases} \tag{7}$$

$$\text{Mode II} \begin{cases} i_s(t_0) = \dfrac{2}{nV_1}(1 - k - 2D_\varphi) \\ i_s(t_2) = \dfrac{2}{nV_1}\left[(k+1)D_\alpha + 2kD_\varphi - 2k\right] \\ i_s(t_3) = \dfrac{2}{nV_1}\left[(1-k)D_\alpha + 2kD_\varphi\right] \end{cases} \tag{8}$$

The average output power can be obtained by solving:

$$P_o = \frac{2}{T_s}\int_0^{\frac{T_s}{2}} \left(v_s(t)\cdot i_s(t)\right)dt \tag{9}$$

The normalized results are listed in the third row of Table I and based on those results, Fig. 3(a) depicts the power ranges of Mode I and Mode II, which are segmented by the blue boundary curve. It can be seen that the output power increases with D_α and D_φ in both modes, and the achievable maximum power of Mode II is larger than that of Mode I. Hence, the DAB converter can operate in Mode I for lower power transmission and Mode II for higher output power.

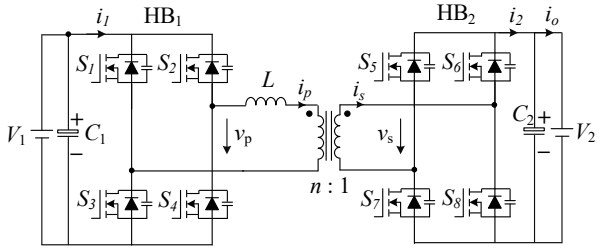

Fig. 1. Dual-active-bridge (DAB) converter topology.

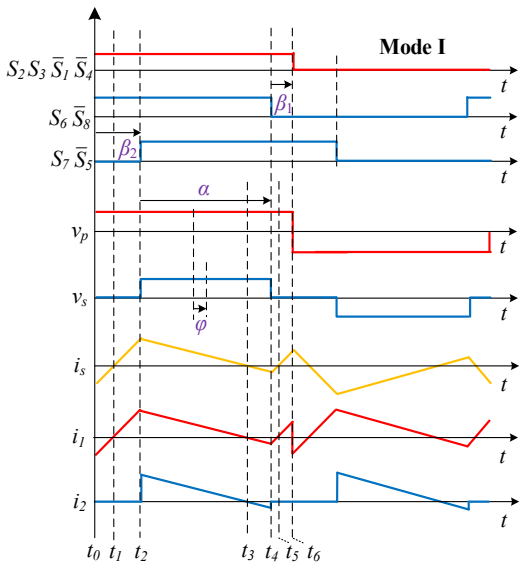

(a)

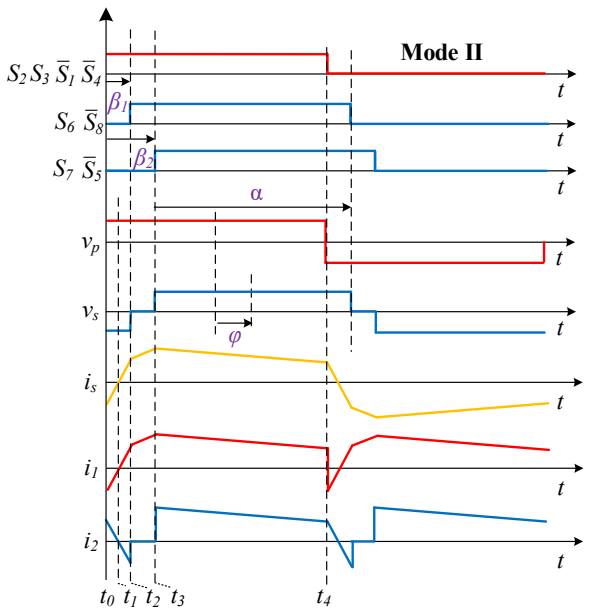

(b)

Fig. 2. Typical waveforms of DAB converters using DPS modulation scheme with k<1 when (a) falling edge of v_s leads v_p (Mode I) (b) falling edge of v_s lags v_p (Mode II)

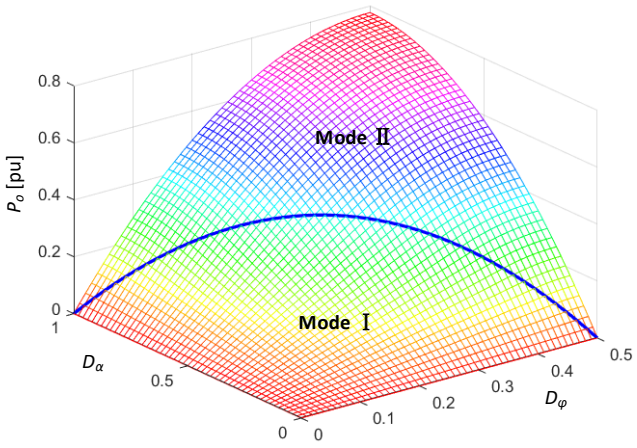

(a)

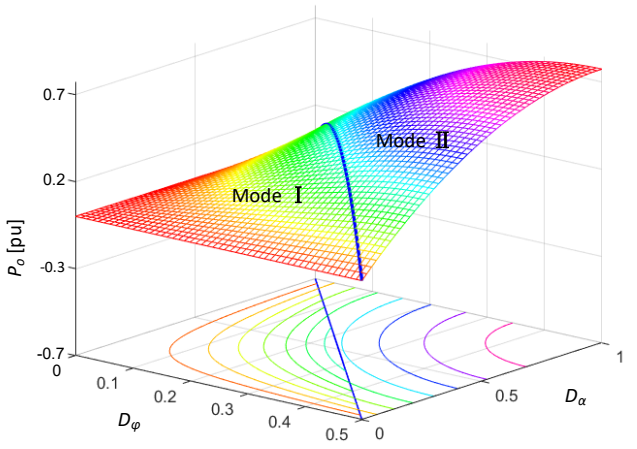

(b)

Fig. 3. 3D plot of the power range as the function of D_α and D_φ with the blue curve as the boundary of Mode I and Mode II (a) front view (b) side view with the contour plane of the output power.

III. Losses Analysis and ZVS Conditions

The power losses of the DAB converter include that of the semiconductor devices and transformer. The auxiliary inductor is taken as a part of the transformer because it functions as an equivalent leakage inductance here. Since every switch conducts current for half of the switching period, the power losses of the switches can be calculated by:

$$P_{sw} = \underbrace{\left(\frac{2}{2}\frac{R_{DSon,p}}{m_p} + \frac{2R_{DSon,s}}{m_s}\right) I_{s,ms}^2}_{\text{conduction losses}} + \underbrace{\frac{2}{2}(t_{d(on),p} + t_{d(on),s}) V_s I_{s,ms} f_s + 2(t_{d(off),p} + t_{d(off),s}) V_s I_{s,ms} f_s}_{\text{switching losses}} \quad (10)$$

where $R_{DSon,p}$, $R_{DSon,s}$ is the on-state resistance of the HB_1, HB_2 transistors, respectively. $I_{s,rms}$ is the root-mean-square value of the secondary transformer current in one switching period:

$$I_{s,\mathrm{rms}} = \sqrt{\frac{1}{T_s}\int_0^{T_s} i_s^2(t)dt} \quad (11)$$

Due to the fact that the body diodes of the transistors only conduct during the dead time to achieve ZVS, the conduction losses of the diodes are neglected since the dead time is usually much shorter than the switching period. Note that if paralleled switches are adopted to reduce the conduction losses and increase the supportable current rating, the number of paralleled switches should also be taken into account, represented by m_p and m_s for HB_1 and HB_2, respectively.

On the other hand, the switching losses of the DAB converters can be estimated according to [17], as marked in (10). $t_{on,p}$, $t_{off,p}$ and $t_{on,s}$, $t_{off,s}$ are the turn-on and turn-off time of the switches S_1~S_4 and S_5~S_8, respectively. Here, $I_{s,dc}$ is the average absolute value of the secondary transformer current, which is calculated by:

$$I_{s.dc} = \frac{1}{T_s}\int_0^{T_s} |i_s(t)|dt \quad (12)$$

For the intermediate high-frequency transformer, the power losses are comprised of two parts: the copper losses of transformer windings and the magnetic core losses. The copper losses can be obtained with:

$$P_{tr,cond} = \left(R_{trs} + \frac{R_{aul} + R_{trp}}{n^2}\right) \cdot I_{s,rms}^2 \quad (13)$$

where R_{aul}, R_{trp} and R_{trs} are the resistances of the auxiliary inductor, primary and secondary winding of the transformer, respectively.

The magnetic core losses are mainly determined by the magnetic flux, the switching frequency, the core volume and the voltage waveform. In order to simplify the core losses calculation, the HF transformer is commonly assumed to be fed with sinusoidal waveforms [18], such that it can be expressed by:

$$P_{tr,core} = k f_s^{\gamma} B^{\sigma} \cdot V_c \quad (14)$$

where k is the material constant, f_s the switching frequency , B the peak flux density and V_c the volume of the magnetic core. γ and σ is the frequency and flux density exponent, respectively, which can be achieved from the core datasheet

TABLE I. EXPRESSIONS AND CONSTRAINTS RELATED TO DAB CONVERTER OPERATION MODES

	Mode I	**Mode II**
Boundary conditions	$0 < D_\alpha \le 1-2D_\varphi$	$1-2D_\varphi < D_\alpha \le 1$
ZVS constraints	$\frac{2k}{1-k} D_\varphi < D_\alpha < k$	$D_\alpha > 2k\left(1-D_\varphi\right)/\left(1+k\right) \quad D_\varphi > \left(1-k\right)/2$
Normalized output power P_o	$4kD_\alpha D_\varphi$	$-k\left(4D_\varphi^2 - 4D_\varphi + \left(1-D_\alpha\right)^2\right)$
Normalized average absolute secondary current $I_{s.dc}$ [pu]	$\left[\left(-k^2+3k-2\right)D_\alpha^2 + \left(-2k^2+2k\right)D_\alpha + \left(-4D_\varphi^2-1\right)k^2 + k^3\right] \Big/ \left(k^2-k\right)$	$\left[\left(-k-1\right)D_\alpha^2 + \left(2k+2\right)D_\alpha + \left(-4D_\varphi^2+8D_\varphi-3\right)k + k^2\right] \Big/ \left(1+k\right)$
Normalized RMS value of the secondary current $I_{s.rms}$ [pu]	$\frac{2}{3}\cdot sqrt\left[3\left(k-2\right)D_\alpha^3 + 9D_\alpha^2 + \left(36D_\varphi^2-9\right)kD_\alpha + 3k^2\right]$	$\frac{2}{3}\cdot sqrt\left[-6D_\alpha^3 + \left(-18kD_\varphi+9k+9\right)D_\alpha^2 + \left(36D_\varphi-18\right)kD_\alpha + 3k^2 - \left(6D_\varphi-3\right)\left(2D_\varphi-1\right)^2 k\right]$

and they are commonly considered as constant for a fixed switching frequency.

Comparing (10), (13) and (14), it can be observed that the semiconductor devices power losses and the transformer conduction losses are closely related to $I_{s,rms}$ and $I_{s,dc}$, whereas the transformer core losses are independent on the load current given by (14). This paper will focus on the effect of $I_{s,rms}$ and $I_{s,dc}$ on the converter losses, thus the magnetic core losses are not studied in this paper.

The selected switch types and measured HF transformer parameters for the DAB converter hardware design are listed in Table II. Due to the high current in the low-voltage output side, each switch of HB_2 is composed of two paralleled MOSFETs with a low on-state resistance. The calculated power losses distribution using (10) and (13) are depicted in Fig. 4, from which it can be seen that the transformer resistive losses contributes a large part of the total power losses, highlighting the necessity to reduce the leakage inductance current.

On the other hand, in order to make all switches achieve zero-voltage switching to improve the converter efficiency and avoid voltage spikes induced by hard-switching, the following conditions (15) and (16) should be satisfied in Mode I and Mode II, respectively:

$$i_s\left(t_0\right) < 0 \quad i_s\left(t_2\right) > 0 \quad i_s\left(t_4\right) < 0 \tag{15}$$

$$i_s\left(t_0\right) < 0 \quad i_s\left(t_2\right) > 0 \quad i_s\left(t_3\right) > 0 \tag{16}$$

Together with (7) and (8), the ZVS conditions can be derived as shown in the second row of Table I. the normalized output power P_o and expressions of normalized $I_{s.dc}$ and $I_{s.rms}$ in operation Mode I and Mode II are summarized in Table I.

IV. OPTIMIZED CONTROL SCHEME FOR LOSSES REDUCTION

Seen from Fig. 3(a), there are different combinations of D_α and D_φ to achieve the same output power in Mode I and Mode II, as the contour plane of the output power shown in Fig. 3(b). Therefore, in order to acquire the optimal combination of D_α and D_φ from the power losses reduction point of view, the formulas of $I_{s.dc}$ and $I_{s.rms}$ regarding with D_α and D_φ are deduced using (11) and (12), as listed in Table I. In order to reduce the power losses consumed by the intermediate HF transformer, the values of $I_{s.dc}$ and $I_{s.rms}$ should be decreased according to (10) and (13).

As the colorful surfaces present, Fig. 5 and Fig. 6 illustrate the relationship between $I_{s.dc}$ or $I_{s.rms}$ and D_α, D_φ for respective Mode I and Mode II using the expressions in Table I. In Mode I, there exist a specific point of (D_α, D_φ) for the minimal $I_{s.dc}$ or $I_{s.rms}$. In Mode II, $I_{s.dc}$ is directly proportional to the value of D_α and D_φ, and the behavior of $I_{s.rms}$ is similar to Mode I. Comparing Fig. 5, Fig. 6 and Fig. 3(b), it can be concluded that the conduction and switching losses can be reduced if the proper combination of D_α and D_φ is applied to the converter for different operating power levels.

TABLE II. COMPONENTS OF THE IMPLEMENTED PROTOTYPE

Components	**Parameters (@T=25°C)**
MOSFETs S_1~S_4: IPW65R080CFD (Infineon)	R_{DSonp} = 72 mΩ
MOSFETs S_5~S_8: 2x IPP110N20N3 (Infineon)	R_{DSons} = 9.6 mΩ
Primary winding of the HF transformer: 35 turns copper foil	R_{trp} = 607.9 mΩ
Secondary winding of the HF transformer: 10 turns copper foil	R_{trs} = 16.5 mΩ
Auxiliary inductor: 10 turns Litz wire, 20 strands, 0.355 mm	R_{aux} = 27.9 mΩ
Magnetic material of the HF transformer	ETD59 ferrite
Magnetic material of the auxiliary inductor	ER42 ferrite

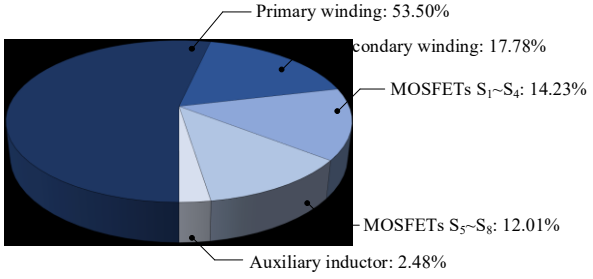

Fig. 4. Caculated losses distribution on the DAB converter components at the output power of 1.5 kW following Table II parameters.

In order to achieve the optimal values of D_α and D_φ for a certain output power, the following equations (17) and (18) can be attained according to the power expressions in Table I, corresponding with Mode I and Mode II.

$$D_\varphi = \frac{P_o}{4kD_\alpha} \tag{17}$$

$$D_\varphi = \frac{k - \sqrt{-k^2 D_\alpha^2 + 2k^2 D_\alpha - kP_o}}{2k} \tag{18}$$

Then by substituting (17) and (18) into the expressions of $I_{s,dc}$ and $I_{s,rms}$, it can be further deduced that when the analytical D_α is equal to the right side of (19) and (20) for Mode I, $I_{s,dc}$ and $I_{s,rms}$ are at their minimum values, respectively.

$$D_{\alpha.dc} = \frac{k\left(1-k+\sqrt{16(1-k)(2-k)D_\varphi^2 + (1-k)^2}\right)}{2(1-k)(2-k)} \tag{19}$$

$$D_{\alpha.rms} = \frac{1-\sqrt{(1-k)^2 - 4k(2-k)D_\varphi^2}}{2-k} \tag{20}$$

Similarly, for operation Mode II, the criteria corresponding to the minimum $I_{s.dc}$ and $I_{s.rms}$ are deduced as (21) and (24), respectively.

$$D_{\alpha.dc} = \frac{2k(1-D_\varphi)}{1+k} \tag{21}$$

Taking into account the ZVS conditions in Table I, the maximum output power for each mode under ZVS can be deduced as:

$$P_{o\max,m1} = 2k^2(1-k) \tag{22}$$

$$P_{o\max,m2} = k \tag{23}$$

where $P_{\text{omax,m1}}$ and $P_{\text{omax.m2}}$ denotes the maximum power of Mode I and Mode II, respectively.

Based on (19), (20), (21), (24), Fig. 7 shows the relationship between D_α and D_φ, where the green curve is for minimized $I_{s.dc}$ and the blue one is for minimized $I_{s.rms}$. Besides, the power curves, the soft-switching area and the boundary of two modes can also be found in the Fig. 7, as displayed by the dashed black curves, the shaded region and the bold line respectively.

The green and blue curves are all within the ZVS area, indicating the minimum $I_{s.dc}$ or $I_{s.rms}$ and ZVS for all DAB switches can be simultaneously achieved. For the power curves, some of them intersect with the green and blue curves in both operation modes, meaning that the power can be reached with minimized $I_{s.dc}$ or $I_{s.rms}$, but it also reveals that the minimization of $I_{s.dc}$ and $I_{s.rms}$ can not be realized at the same time. Furthermore, there are some other power curves separated from minimized $I_{s.dc}$, which can be observed in mode II, implying that the optimal $I_{s.dc}$ can not be reached when the converter works on these power levels. In other words, the switching losses on the semiconductor devices can not be minimized considering (10).

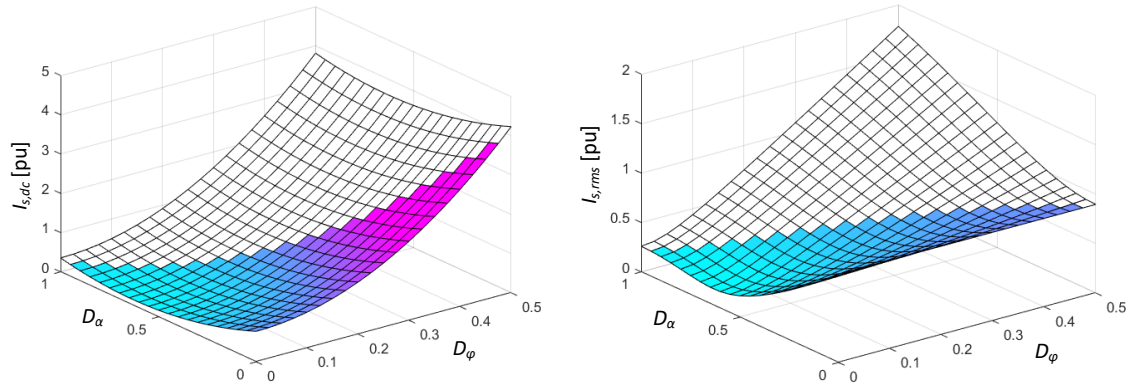

(a) (b)

Fig. 5. $I_{s,dc}$ and $I_{s,rms}$ versus D_α and D_φ for operation Mode I: (a) Plane of $I_{s,dc}$ regarding to D_α and D_φ (b) Plane of $I_{s,rms}$ regarding to D_α and D_φ

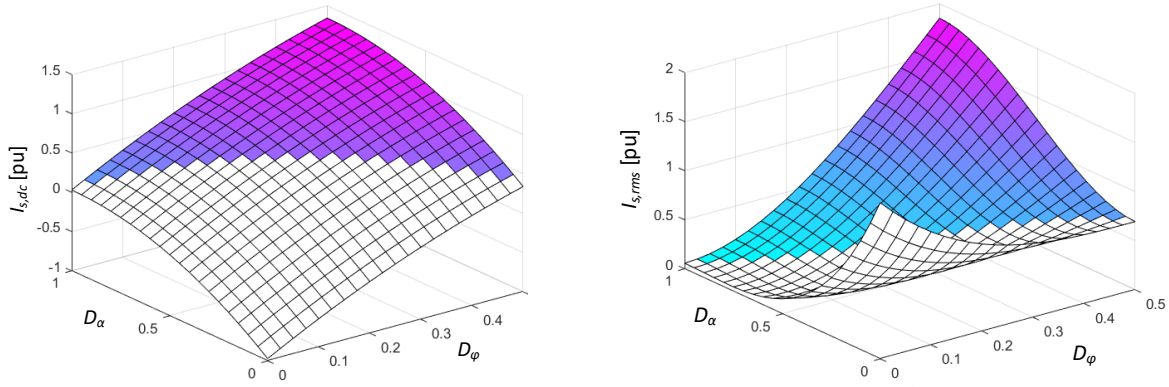

(a) (b)

Fig. 6. $I_{s,dc}$ and $I_{s,rms}$ versus D_α and D_φ for operation Mode II: (a) Plane of $I_{s,dc}$ regarding to D_α and D_φ (b) Plane of $I_{s,rms}$ regarding to D_α and D_φ

$$D_{\alpha.rms}=\begin{cases}\dfrac{2D_\varphi+k-1+\sqrt{4\left(k^2+1\right)D_\varphi^2-4\left(k^2-k+1\right)D_\varphi+2k^2-2k+1}}{k}, & \dfrac{1-k}{2}<D_\varphi<\dfrac{k-1+\sqrt{1-k^2}}{2k}\\ 1, & \dfrac{k-1+\sqrt{1-k^2}}{2k}<D_\varphi<0.5\end{cases} \tag{24}$$

Seen from (19), (20), (21), (24), the relationship between D_α and D_φ is segmented and complicated depending on the operation modes and the value of D_φ, which is the root cause of complexity for the minimization of $I_{s.dc}$ or $I_{s.rms}$. In order to simplify the control procedure, a uniform control method is plotted in Fig. 7 using quadratic curve fitting technique, as the red curve presents, which is formulated as:

$$D_{\alpha.opt}=\frac{4(3k-2)}{k(k-2)}D_\varphi^2+\frac{2(2k-1)}{k}D_\varphi+\frac{k}{2-k} \tag{25}$$

Thus the value of D_α and D_φ can be calculated from (25) in both modes, and meanwhile the ZVS conditions are also satisfied as the whole control curve is located in the ZVS area. Besides, it can be seen that all power curves have intersections with the red curve, which indicates a wide power range of the uniform control.

In order to evaluate the effect of the control method on the losses reduction, the simulated total power losses P_{tot} for different output powers are depicted in Fig. 8. The operation state of the DAB converter is determined by the intersection points of the power curve and control curves. Taking Mode I as an example, the DAB converter is controlled by combination (D_α, D_φ) at the operation point B_1, B_2, B_3, B_4 shown in Fig. 7, where no optimization, minimized $I_{s.dc}$ control minimized $I_{s.rms}$ control and the uniform control are employed, respectively. By comparing the simulation results in Fig. 8, the proposed uniform control can effectively reduce the power losses compared to the nonoptimized method and further achieve almost the same power losses as that when the minimized $I_{s.dc}$ or $I_{s.rms}$ is satisfied.

The block diagram of the proposed uniform control scheme for a DAB converter is illustrated in Fig. 9. The operation mode is firstly selected by comparing the given power with the maximum power of each mode, as defined in (22) and (23). Next the actual transmission power P_o is

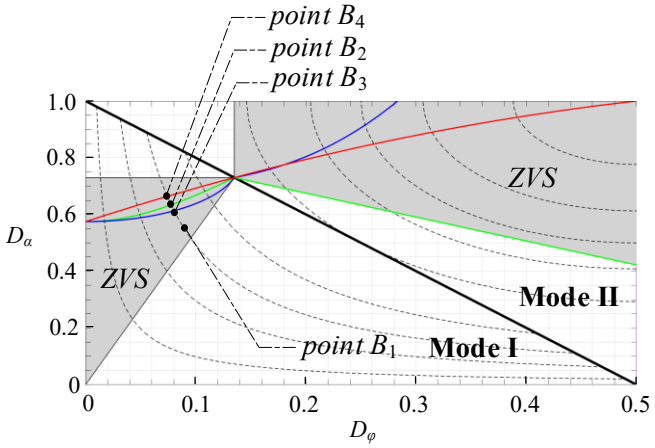

Fig. 7. Curves of different control schemes

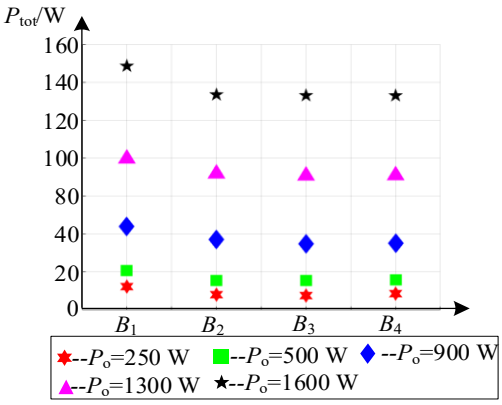

Fig. 8. Simulated total power losses under different control schemes

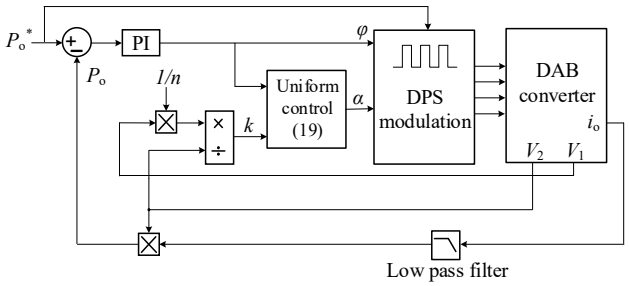

Fig. 9. Block diagram of the proposed uniform control

calculated by multiplying V_2 with the average value of the output current i_o, which can be obtained through a low pass filter. Then the error between the reference value P_o^* and actual P_o is used to produce the phase-shift angle φ between the two full bridges. After the calculation of the voltage ratio k, the other angle α can be achieved using (25). Finally, the two angles are applied to the DPS modulation module and the suitable switching signals are generated.

V. Experimental Verification

An experimental platform for the DAB converter is implemented to validate the proposed uniform control, as shown in Fig. 10. The system parameters are summarized in Table III. The steady state waveforms of the DAB converter in operation Mode I are illustrated in Fig. 11, where v_p and v_s are voltage waveforms generated by HB_1 and HB_2, and i_p, i_s are the primary and secondary transformer current, respectively. Fig. 11(a) shows the measured waveforms when the DAB converter works without adopting any optimal control, which is corresponding to the operation point B_1 in Fig. 7. Fig. 11(b) shows the working waveforms when the converter is modulated by the proposed uniform control, corresponding to the operation point B_4. The output power for both operation points is given at 150 W. As marked in the figure, the value of $I_{s.dc}$ and $I_{s.rms}$ in Fig. 11(b) are both lower than in Fig. 11(a), indicating the effectiveness of the uniform control in reducing the conduction and switching losses of the DAB converter.

TABLE III. PARAMETERS FOR EXPERIMENT

Parameters	Values
High voltage side V_1	190 V
Low voltage side V_2	70 V
Turns ratio of the HF transformer n:1	3.5:1
Switching frequency f_s	60 kHz
Dead time T_{dead}	200 ns
Series inductor L	36.2 μH
Primary side leakage inductance L_{trp}	4.5 μH
Secondary-side leakage inductance L_{trs}	372.5 nH
Primary DC capacitor C_1	0.78 mF
Secondary DC capacitor C_2	1.5 mF

Moreover, Fig. 12 presents the obtained results when the converter works in operation Mode II with a transmission power of 1000 W. The $I_{s.rms}$ in Fig. 12(a) and Fig. 12(b) are 21.95 A and 16.74 A, respectively, and the calculated $I_{s.dc}$ are respective 19.55 A and 14.64 A. Similarly, the lower $I_{s.rms}$ and $I_{s.dc}$ in Fig. 12(b) also validates that the proposed uniform control has a better performance in reducing the converter power losses . Besides, by operating the DAB converter with different transmission power, Fig. 13 plots the measured efficiency curves of the whole system, where blue represents the operation without optimal control and red denotes the uniform control. It can be seen that the system efficiency is improved in the entire power range, especially at light load condition.

In order to evaluate the dynamic response of the proposed uniform control scheme, the DAB converter is controlled to switch between two modes with different given power. The waveforms of the output voltage V_2, the primary voltage v_p, the output current I_o and the output power P_o are measured and displayed in Fig. 14.

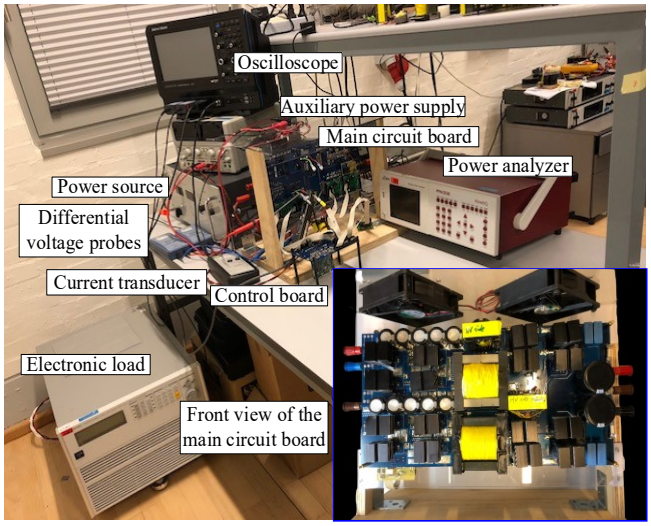

Fig. 10. Test platform for the DAB converter

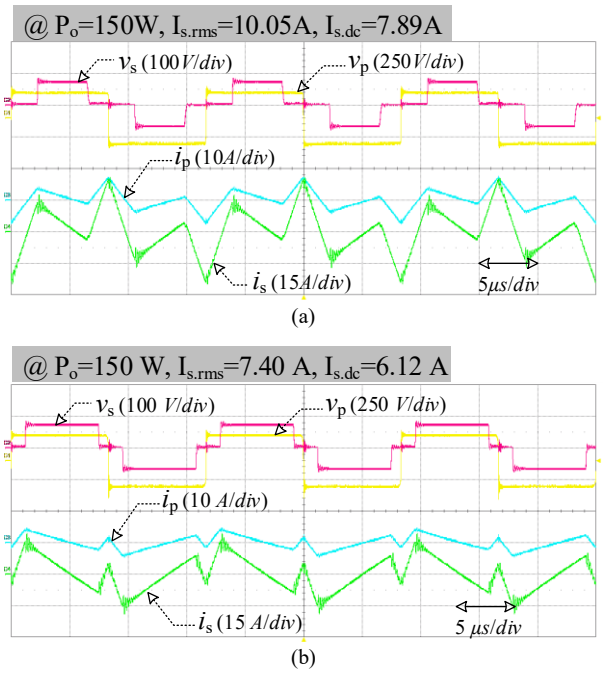

Fig. 11. Obtained experimental waveforms of DAB converter in operation Mode I: (a) without optimal control (b) with uniform control

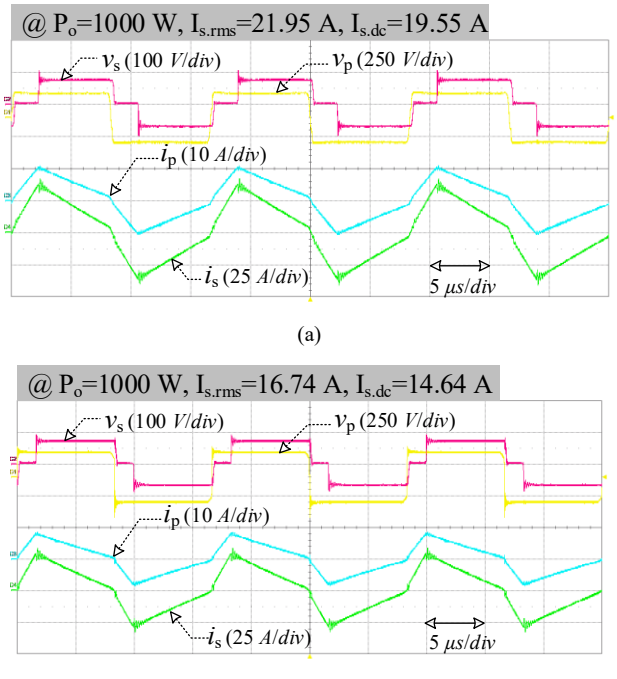

Fig. 12. Obtained experimental waveforms of DAB converter in operation Mode II: (a) without optimal control (b) with uniform control

The output power is obtained by multiplying the output voltage and output current, which can be realized using the math function of the oscilloscope. The output power is boosted from 460 W to 1120 W at the instant as the blue line shows in Fig. 14(a) and then it is lowered back to 460 W as shown in Fig. 14(b). The DAB converter can automatically switch to the proper operation Mode under the uniform control, which is determined by the given output power. Besides, it can be seen that the DAB converter can reach the new steady state extremely fast after the change of the reference output power.

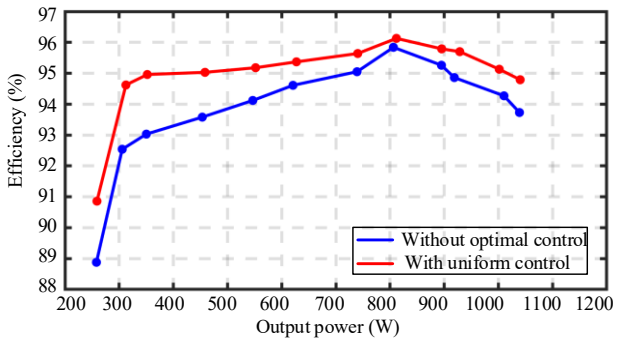

Fig. 13. Measured efficiencies currves of the DAB converter for different output powers

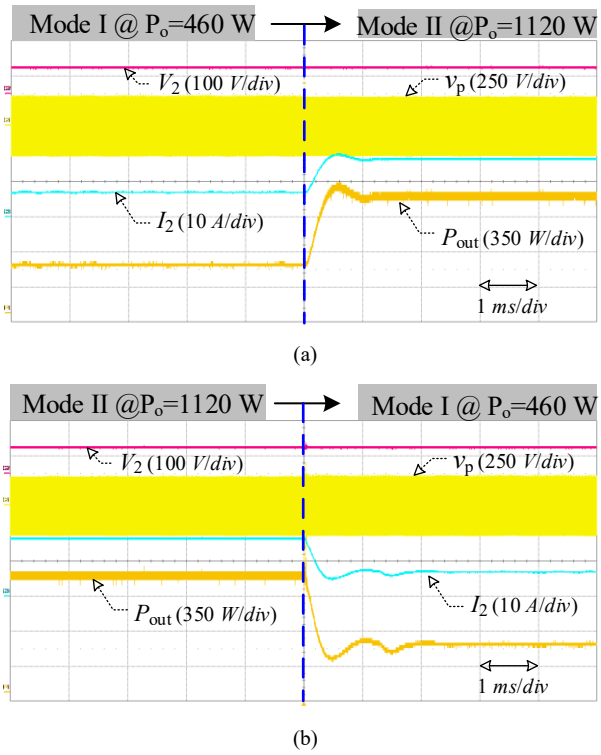

Fig. 14. Dynamic response waveforms of the DAB converter with the output power: (a) inceased from 460W to 1120W (b) decreased from 1120W to 460W

VI. Conclusions

This paper proposes a uniform control scheme to reduce the conduction and switching losses of the DAB converter based on the DPS modulation. Compared to the conventional control methods, the proposed uniform control can not only effectively reduce the switching and conduction losses, which is reflected by the improved converter efficiency, but also lower the control complexity by rearranging the switching signals based on the uniform selection of the control variables in both operation modes. Moreover, the dynamic response of the DAB converter to the change of the output power can be also improved due to the simplified and unified control scheme. Besides, the zero-voltage switching is also guaranteed for all switches in a wide voltage range.

References

[1] G. Ortiz, C. Gammeter, J. W. Kolar, and O. Apeldoorn, "Mixed MOSFET-IGBT bridge for high-efficient medium-frequency dual active-bridge converter in solid state transformers," in *IEEE Workshop on Control and Modeling for. Power Electronics*, 2013, pp. 1–8.

[2] S. Anwar, W. Zhang, F. Wang, and D. J. Costinett, "Integrated dc-dc converter design for electric vehicle powertrains," in *IEEE Applied Power Electronics Conference and Exposition*, 2016, pp. 424–431.

[3] S. P. Engel, M. Stieneker, N. Soltau, S. Rabiee, H. Stagge, and R. W. D. Doncker, "Comparison of the modular multilevel dc converter and the dual-active bridge converter for power conversion in HVDC and MVDC grids," *IEEE Transactions on Power Electronics*, vol. 30, no. 1, pp. 124–137, Jan. 2015.

[4] B. Zhao, Q. Yu, and W. Sun, "Extended-phase-shift control of isolated bidirectional dc-dc converter for power distribution in microgrid," *IEEE Transactions on Power Electronics*, vol. 23, no. 6, pp. 2905–2914, Nov. 2008.

[5] H. Bai and C. Mi, "Eliminate reactive power and increase system efficiency of isolated bidirectional dual-active-bridge dc-dc converters using novel dual-phase-shift control," *IEEE Transactions on Power Electronics*, 2009, pp. 455–452.

[6] F. Li, Y. Li and X. You, "Optimal dual-phase-shift control strategy of an isolated buck–boost converter with a clamped inductor, " *IEEE Transactions on Power Electronics*, vol. 33, no. 6, pp. 5374–5385, Jun. 2018.

[7] K. Wu, C. W. De Silva, and W. G. Dunford, "Stability analysis of isolated bidirectional dual active full-bridge DC-DC converter with triple phase shift control," *IEEE Transactions on Power Electronics*, vol. 27, no. 4, pp. 2007-2017, Apr. 2012.

[8] A. Taylor, G. Liu, H. Bai, A. Brown, P. Johnson and M .McAmmond, "Multiple-phase-shift control for a dual active bridge to secure zero-voltage switching and enhance light-load performance," *IEEE Transactions on Power Electronics*, vol. 33, no. 6, pp. 4584-4588, Jun. 2018.

[9] J. Zhang, J. Lai, R. Kim and W. Yu, " High-power density design of a soft-switching high-power bidirectional dc–dc converter," *IEEE Transactions on Power Electronics*, vol. 22, no. 4, pp. 1145–1153, Jul. 2007.

[10] J. Everts, J. Van den Keybus, F. Krismer, J. Driesen, and J. W. Kolar, "Switching control strategy for full ZVS soft-switching operation of a dual active bridge AC/DC Converter," in *IEEE Applied Power Electronics Conference and Exposition*, 2012, pp. 1048-1055.

[11] H. Zhou and A. Khambadkone, "Hybrid modulation for dual-active bridge bidirectional converter with extended power range for ultracapacitor application," *IEEE Transactions on Industry Applications*, vol. 45, no. 4, pp. 1434-1442, Jul.-Aug. 2009.

[12] A. K. Jain and R. Ayyanar, "PWM control of dual active bridge: Comprehensive analysis and experimental verification," *IEEE Transactions on Power Electronics*, vol. 26, no. 4, pp. 1215-1227, Apr. 2011.

[13] G. Oggier and M. Ordonez, "High efficiency DAB converter using switching sequences and burst-mode," *IEEE Transactions on Power Electronics*, vol. 31, no. 3, pp. 2069-2082, Mar. 2016.

[14] P. Davari, Y. Yang, F. Zare and F. Blaabjerg, "A review of electronic inductor technique for power factor correction in three-phase adjustable speed drives," in *IEEE Energy Conversion Congress and Exposition* , 2016, pp. 1-8.

[15] L. Wang, Q. Zhu, W. Yu and A. Huang, "A medium-voltage medium-frequency isolated DC–DC converter based on 15-kV SiC MOSFETs," *IEEE Journal of Emerging and Selected Topics in Power Electronics*, vol. 5, no. 1, pp. 100-109, Mar. 2017.

[16] F. Xue, R. Yu and A. Huang, "A 98.3% efficient GaN isolated bidirectional DC–DC converter for DC microgrid energy storage system applications," *IEEE Transactions on Industrial Electronics*, vol. 64, no. 11, pp. 9094 – 9103, Nov. 2017.

[17] S.Rahman, F. Stückler and K. Siu, "PFC boost converter design guide," Available online at https://www.infineon.com.

[18] W. A. Roshen, "A practical, accurate and very general core loss model for nonsinusoidal waveforms," *IEEE Transactions on Power Electronics*., vol. 22, no. 1, pp. 30–40, Jan. 2007.